Acta Crystallographica Section D
Biological Crystallography
ISSN 1399-0047

Structure determination of human Fas apoptosis inhibitory molecule and identification of the critical residues linking the interdomain interaction to the anti-apoptotic activity

Guoming Li,[a]‡ Linglong Qu,[a,b]‡ Shuaipeng Ma,[b,c] Yujie Wu,[b,c] Changwen Jin[b,c]* and Xiaofeng Zheng[a,b]*

[a]State Key Laboratory of Protein and Plant Gene Research, Peking University, Beijing 100871, People's Republic of China, [b]Department of Biochemistry and Molecular Biology, School of Life Sciences, Peking University, Beijing 100871, People's Republic of China, and [c]Beijing Nuclear Magnetic Resonance Center, Peking University, Beijing 100871, People's Republic of China

‡ These authors contributed equally to this work.

Correspondence e-mail: changwen@pku.edu.cn, xiaofengz@pku.edu.cn

Received 2 July 2013
Accepted 3 March 2014

PDB references: FAIM-S, NTD, 3mx7; CTD, 2kw1

Fas apoptosis inhibitory molecule (FAIM) is a highly conserved anti-apoptotic protein which plays important roles in cells. There are two isoforms of FAIM, of which the short isoform FAIM-S is broadly expressed in all tissues, whereas the long isoform FAIM-L is exclusively expressed in the nervous system. No structure of human FAIM has been reported to date and the detailed molecular mechanisms underlying the anti-apoptotic function of FAIM remain unknown. Here, the crystal structure of the human FAIM-S N-terminal domain (NTD) and the NMR solution structure of the human FAIM-S C-terminal domain (CTD) were determined. The structures revealed that the NTD and CTD adopt a similar protein fold containing eight antiparallel β-strands which form two sheets. Both structural and biochemical analyses implied that the NTD exists as a dimer and the CTD as a monomer and that they can interact with each other. Several critical residues were identified to be involved in this interaction. Moreover, mutations of these critical residues also interfered in the anti-apoptotic activity of FAIM-S. Thus, the structural and functional data presented here will provide insight into the anti-apoptotic mechanism of FAIM-S.

1. Introduction

Cell death is an essential ingredient of life. As the main form of cell death, apoptosis constitutes the physiological route to eliminate damaged or infected cells in order to maintain homeostasis. The subtle molecular mechanisms involved in its execution and regulation have been well characterized. Among these, the Fas-induced apoptosis signalling pathway services as a key player in the regulation of immune responses and tumour suppression (Trauth *et al.*, 1989; Yonehara *et al.*, 1989; Suda *et al.*, 1995; Chinnaiyan *et al.*, 1996; Oshimi *et al.*, 1996; Smyth *et al.*, 1996). Activation of Fas by its physiological ligand FasL can stimulate the recruitment of the adapter protein FADD (Fas-associated protein with death domain) through a homotypic interaction with the death domain. Subseqently, the initiator caspase pro-caspase 8 is recruited into the death-inducing signalling complex (DISC) and then processed, which activates a downstream effector caspase and triggers apoptosis (Alderson *et al.*, 1995; Brunner *et al.*, 1995; Fisher *et al.*, 1995). Several anti-apoptotic proteins, such as Bcl-xL and c-FLIP, can modulate this signalling pathway, and overexpression of these proteins has been reported to protect primary B cells from Fas killing (Grillot *et al.*, 1996; Schneider *et al.*, 1997; Van Parijs *et al.*, 1999; Wang *et al.*, 2000).

A novel gene encoding the Fas apoptosis inhibitory molecule (FAIM) was first identified in Fas-resistant primary B cells (Schneider *et al.*, 1999). The anti-apoptotic function of FAIM has also been demonstrated in FAIM-transfected cells

Table 1
Data-collection and refinement statistics for the FAIM-S NTD.

Values in parentheses are for the highest resolution shell.

Data-collection statistics	
Space group	$P3_121$
Unit-cell parameters (Å, °)	$a = b = 58.02$, $c = 71.11$, $\alpha = \beta = 90$, $\gamma = 120$
Wavelength (Å)	0.9798
Resolution range (Å)	50.0–1.76 (1.82–1.76)
Total No. of reflections	143917
No. of unique reflections	12989
Completeness (%)	99.7 (99.4)
$R_{\rm merge}$† (%)	6.9 (18.7)
Multiplicity	5.7 (5.0)
Mean $I/\sigma(I)$	17.3 (11.0)
Refinement statistics	
No. of reflections used	12781
No. of reflections in test set	1078
$R_{\rm work}$‡ (%)	17.6
$R_{\rm free}$‡ (%)	20.1
Mean B factor (Å^2)	20.4
R.m.s.d., bond distances (Å)	0.017
R.m.s.d., bond angles (°)	1.741
Ramachandran plot, residues in (%)	
Most favoured regions	95
Additional allowed regions	5
Generously allowed regions	0
Disallowed regions	0

† $R_{\rm merge} = \sum_{hkl}\sum_i |I_i(hkl) - \langle I(hkl)\rangle| / \sum_{hkl}\sum_i I_i(hkl)$, where $I_i(hkl)$ is an individual intensity measurement and $\langle I(hkl)\rangle$ is the average intensity for all i observations of reflection hkl. ‡ $R_{\rm work} = \sum_{hkl} ||F_{\rm obs}| - |F_{\rm calc}|| / \sum_{hkl} |F_{\rm obs}|$, where $F_{\rm obs}$ and $F_{\rm calc}$ are the observed and calculated structure-factor amplitudes, respectively. $R_{\rm free}$ is defined as $R_{\rm work}$ for a randomly selected subset of reflections.

(Schneider *et al.*, 1999; Nicholson *et al.*, 1995; Tewari *et al.*, 1995). The *faim* gene localizes to human chromosome 3q22, which is a cytogenetic region correlated with diseases (Zhong *et al.*, 2001; Hemond *et al.*, 2009). Some abnormalities in this region have been found to be associated with a number of types of human cancers, suggesting a possible role of FAIM in oncogenesis (Petersen *et al.*, 1997). FAIM is highly evolutionarily conserved and broadly expressed, suggesting that it may play a key role in physiological function (Schneider *et al.*, 1999). An alternative spliced form of FAIM containing 22 extra residues at the N-terminus has been characterized in brain and is named FAIM-Long (FAIM-L), whereas the original FAIM is termed FAIM-Short (FAIM-S) (Zhong *et al.*, 2001). FAIM-L is exclusively expressed in the nervous system and protects primary neurons against death receptor-induced apoptosis (Segura *et al.*, 2007), thus playing a different role from FAIM-S, which promotes neurite outgrowth through the ERK and NF-κB pathways (Sole *et al.*, 2004). FAIM-S has also been reported to enhance CD40-mediated signal transduction and to regulate B-cell differentiation (Kaku & Rothstein, 2009*a*,*b*).

FAIM-S is composed of two independent folding domains: the N-terminal domain (NTD; residues 1–90) and the C-terminal domain (CTD; residues 91–179). NMR analysis of the murine FAIM-S CTD indicates that the NTD interacts with the CTD in certain contexts (Hemond *et al.*, 2009), but the exact mechanism and its consequences still remain unclear. Because there is no remarkable sequence homology between FAIM-S and any protein of known structure except for the murine FAIM-S CTD, experimental structure determination is necessary to help us to further understand the precise molecular function of FAIM-S in the cell.

Here, we report the crystal structure of the human FAIM-S NTD and the NMR solution structure of the FAIM-S CTD, and analyze the interaction between the NTD and the CTD of FAIM-S. We also identify the residues that are involved in the interaction and that are critical for the anti-apoptotic activity of FAIM-S. Our study provides structural and functional information on FAIM-S and suggests a possible molecular mechanism of FAIM-S in the regulation of apoptosis.

2. Materials and methods

2.1. Plasmid construction

The sequences encoding FAIM-S, the FAIM-S NTD (residues 1–90) and the FAIM-S CTD (residues 91–179) were amplified and cloned into pET-28a vector. Full-length or fragments of FAIM-S and their corresponding variants including E38A, R110A or N123A mutations introduced by overlap extension PCR were cloned into pcDNA3-3Flag and pcDNA3-3Myc vectors. Fas, Bax and caspase 9 were cloned into pCMV-HA vector.

2.2. Protein expression and purification

The expression and purification of the FAIM-S NTD and the FAIM-S CTD were performed following the procedure described previously (Li *et al.*, 2010). Selenium-labelled FAIM-S NTD was overexpressed in *Escherichia coli* strain B834. The expression clones were cultured in 20 ml Luria–Bertani medium containing kanamycin (50 µg ml^{-1}) at 310 K overnight and then transferred into 1 l fresh M9 medium and cultured at 310 K continuously. When the $OD_{600\ nm}$ reached 0.6–0.8, 0.5 mM isopropyl β-D-1-thiogalactopyranoside (IPTG) was added to induce expression of the FAIM-S NTD. Meanwhile, selenomethionine was added for incorporation into the recombinant protein. After culture at 291 K for 20 h, the cells were harvested by centrifugation at 5000 rev min^{-1} for 10 min. Purification of the selenium-labelled protein followed the same procedure as described above. The purity of all proteins was greater than 95% as confirmed by SDS–PAGE.

2.3. Protein crystallization of the FAIM-S NTD

Both native and selenium-labelled NTDs were crystallized at 293 K by the hanging-drop vapour-diffusion method using screening kits from Hampton Research. Each drop was prepared by mixing 1.2 µl protein solution with 1.2 µl reservoir solution and was allowed to reach equilibrium over 300 µl reservoir solution. After optimizing the pH, buffer, protein concentration, precipitant and temperature, crystals with a diamond shape (0.5 × 0.4 × 0.2 mm) that yielded the best diffraction quality were obtained within 7 d from a reservoir solution at pH 6.5 consisting of 0.67 M sodium phosphate, 0.73 M potassium phosphate with a protein concentration of 19 mg ml^{-1}.

2.4. Diffraction data collection and processing of the FAIM-S NTD

Prior to data collection, crystals were transferred into the corresponding reservoir solution containing 20% glycerol as a cryoprotectant. The crystals were flash-cooled in a liquid-nitrogen stream at 100 K. A data set for the native NTD was collected at 100 K on beamline 3W1A at Beijing Synchrotron Radiation Facility. The crystal belonged to space group $P3_121$, with unit-cell parameters $a = b = 58.02$, $c = 71.11$ Å, $\alpha = \beta = 90$, $\gamma = 120^\circ$. In order to solve the phase problem for the protein, crystals of the selenomethionyl (SeMet) derivative were prepared. Data sets for the SeMet derivative of the NTD were collected at 100 K on beamline BL17U1 at Shanghai Synchrotron Radiation Facility. The SeMet-derivative crystal belonged to the same space group as the native crystal and had similar unit-cell parameters. All data were processed, integrated, scaled and merged using *HKL*-2000 (Otwinowski & Minor, 1997). The data-collection statistics are shown in Table 1.

2.5. Phasing, model building and refinement

The structure of the FAIM-S NTD was solved by the single-wavelength anomalous dispersion (SAD) method from a SeMet derivative of the NTD. Three Se atoms were located in the NTD and initial phases were calculated by the program *SOLVE* (Terwilliger & Berendzen, 1999). Density modification (solvent flipping) and phase extension to 1.76 Å resolution was performed using *RESOLVE* (Terwilliger, 2000). The model of the NTD was automatically traced using *ARP*/*wARP* (Perrakis *et al.*, 1999) with approximately 80% completeness. The structure was built further manually and refined using *Coot* (Emsley *et al.*, 2010) and *REFMAC* (Murshudov *et al.*, 2011). The FAIM-S NTD crystal structure was refined at 1.76 Å resolution to a final $R_{\rm work}$ of 0.1756 and $R_{\rm free}$ of 0.2005. Validation of all final models was carried out with *PROCHECK* (Laskowski *et al.*, 1996). Electrostatic surface charges were generated by *APBS* (Baker *et al.*, 2001). All figures were prepared with *PyMOL* (http://www.pymol.org/). The final refinement statistics are summarized in Table 1.

2.6. NMR sample preparation of the FAIM-S CTD

Uniformly ^{15}N/^{13}C-labelled and ^{15}N-labelled proteins were overexpressed in *E. coli* strain BL21 (DE3) at 310 K in M9 minimal medium containing ^{15}N-labelled ammonium chloride in the presence or absence of ^{13}C-labelled glucose, respectively. The labelled proteins were purified using the same protocol as used for the unlabelled FAIM-S CTD. The purity was also greater than 95% as confirmed by SDS–PAGE. NMR samples were prepared in a buffer at pH 7.0 consisting of 10 m*M* HEPES, 25 m*M* NaCl, 5 m*M* DTT in 90% H_2O/10% D_2O; 2,2-dimethyl-2-silapentane-5-sulfonic acid (DSS) was added as an internal chemical shift reference. NMR samples with a protein concentration of about 1 m*M* were used for structure determination.

2.7. NMR spectroscopy of the FAIM-S CTD

NMR experiments were carried out at 294 K on Bruker Avance 500 and 800 MHz spectrometers equipped with four RF channels and triple resonance cryo-probes with pulsed-field gradients. Three-dimensional triple-resonance HNCA, HN(CO)CA, HNCACB, CBCA(CO)NH, HBHA(CO)NH, HNCO and HN(CA)CO spectra were collected to obtain the backbone resonance assignments. Three-dimensional H(CC)(CO)NH-TOCSY, (H)CC(CO)NH-TOCSY, HCCH-TOCSY, CCH-TOCSY, HCCH-correlation spectroscopy (COSY), CCH-COSY and ^{15}N-edited TOCSY-HSQC spectra were recorded for the side-chain resonance assignments. Three-dimensional ^{15}N- and ^{13}C-edited nuclear Overhauser effect spectroscopy (NOESY)-HSQC (mixing times of 100 and 50 ms) experiments were performed to confirm the assignments and to generate distance restraints for structure calculations. All NMR data were processed using *NMRPipe* (Delaglio *et al.*, 1995) and analyzed using *NMRView* (Johnson, 2004).

2.8. Structure calculations

NMR structures of the FAIM-S CTD were calculated using NOE-derived distance restraints in combination with dihedral angle restraints. The backbone dihedral angle restraints were determined using the program *TALOS* (Cornilescu *et al.*, 1999). The initial structures of the CTD were calculated using the *CANDID* module of *CYANA* using NOE-derived distance restraints and dihedral angle restraints (Güntert *et al.*, 1997; Herrmann *et al.*, 2002). Firstly, 50 structures were calculated and the ten structures with the lowest target function values were selected as the filter models. The program *SANE* was employed to obtain further assignments semi-automatically from three-dimensional NOESY spectra based on the chemical shift assignments and predicted secondary-structure information (Duggan *et al.*, 2001). The distance restraints subsequently generated by *SANE* were used as input for the structure calculations by *CYANA*. A total of 200 structures were calculated using *CYANA*. The 100 structures with the lowest target function values were selected and refined by *AMBER*7 using the ff99 force field and the generalized Born solvation model. A 30 ps simulated annealing from 1000 to 0 K was performed. The force constants for the NOE distance and the dihedral angle restraints were 20 kcal mol^{-1} Å^{-2} and 50 kcal mol^{-1} rad^{-2}, respectively. Chirality and transpeptide ω restraints with force constants of 150 kcal mol^{-1} rad^{-2} and 50 kcal mol^{-1} rad^{-2}, respectively, were added to prevent chirality inversions or peptide-bond flips during the high-temperature portions of simulated annealing. In the process of structure calculation, several iterations of *SANE–CYANA–AMBER* were performed in conjunction with manual violation analysis. Finally, the 20 structures with the lowest *AMBER* energies were selected to represent the CTD. The program *PROCHECK_NMR* was used to analyze the stereochemical geometry by Ramachandran statistics (Laskowski *et al.*, 1996).

2.9. Cells and reagents

Human embryonic kidney 293T (HEK 293T) cells were cultured in Iscover's modified Dulbecco's medium (IMDM, Gibco) supplemented with 10%(*v*/*v*) foetal calf serum (Hyclone) at 310 K in 5% CO_2. The transfection reagent MegaTran 1.0 was from OriGene. Monoclonal anti-Flag (M2; F3165) was from Sigma and anti-Myc (PL14; M047-3) was from MBL. RDye 800CW secondary antibody was from LI-COR Biosciences. The Apoptosis Detection Kit was from KeyGen.

2.10. Co-immunoprecipitation and immunoblot analysis

Cells were harvested after 48 h of transfection and were lysed for 2 h at 277 K in lysis buffer (50 m*M* Tris–HCl pH 8.0, 1.0% Nonidet P-40, 1 m*M* EDTA, 150 m*M* NaCl, 1 m*M* phenylmethylsulfonyl fluoride, 1 mg ml^{-1} leupeptin, 1 mg ml^{-1} aprotinin, 1 mg ml^{-1} pepstatin). Lysates were centrifuged for 15 min at 13 000 rev min^{-1} and the supernatant was incubated with the corresponding antibodies overnight at 277 K. Protein G Sepharose was added and the samples were incubated for 4 h. The Sepharose beads were washed three times with lysis buffer, and precipitated proteins were fractionated by SDS–PAGE and transferred to nitrocellulose membranes (GE Healthcare). Membranes were blocked in 5%(*w*/*v*) nonfat milk in PBS containing 0.1%(*v*/*v*) Tween 20 and probed with primary and secondary antibodies as indicated. An immunoblot analysis was performed and the protein signals were detected and quantified using the Odyssey Infrared Imaging System and the *Odyssey* v.3.0 software (LI-COR Biosciences).

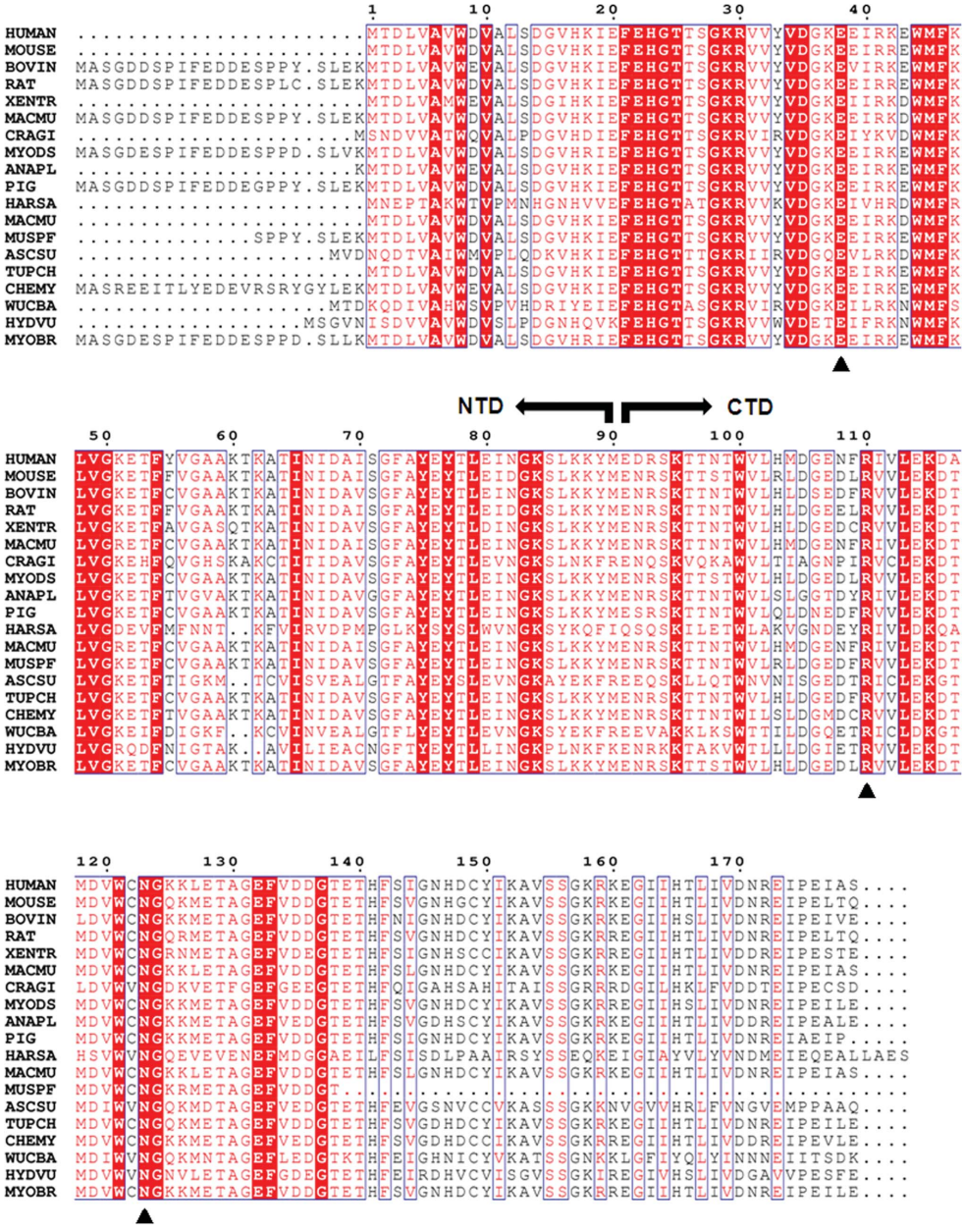

Figure 1
Alignment of selected FAIM sequences among different organisms. Identical residues are boxed and coloured according to the degree of substitution at each position. Numbering is performed according to human FAIM-S. The arrows indicate the two half truncations of FAIM-S, NTD and CTD, used in the study. The triangles show the most conserved residues (Glu38, Arg110 and Asn123) on which we focused in the experiments. The sequence alignment was generated using *MUSCLE* (Edgar, 2004) and presented using *ESPript* (Gouet *et al.*, 1999).

2.11. Apoptosis assay

Cells were transfected with wild-type FAIM-S or the full-length mutation constructs E38A, R110A or N123A together with plasmids encoding Bax, Fas or caspase 9. 1 × 10^5 cells were suspended in 500 µl binding buffer after 48 h of transfection and 5 µl Annexin V-FITC and 5 µl propidium iodide were added. The mixture was incubated for 15 min at room temperature in the dark. The cells were then subjected to flow cytometry to measure the apoptosis rate (%) with a FACS-Calibur cytometer (Becton Dickinson). All data were expressed as mean values ± standard deviation (SD). Statistical analysis was performed using one-way analysis of variance followed by Student's *t*-test.

3. Results and discussion

3.1. Overall structures of the FAIM-S NTD and CTD

Sequence alignment of human FAIM-S with selected FAIMs from publicly available databases indicated that FAIM-S is highly evolutionarily conserved across a broad phylogenetic chasm (Fig. 1). To interpret the molecular mechanism of the regulatory function of FAIM-S, we first tried to determine the crystal structure of full-length FAIM-S. However, as mentioned previously (Li *et al.*, 2010), full-length FAIM-S after purification tended to degrade into two bands within 2 d, which prevented it from crystallizing. Therefore, two half truncations of FAIM-S, the NTD (1–90) and the CTD (91–179) (Fig. 1), were designed to obtain more stable proteins. The structures of the NTD and the CTD were determined by X-ray crystallography and NMR, respectively.

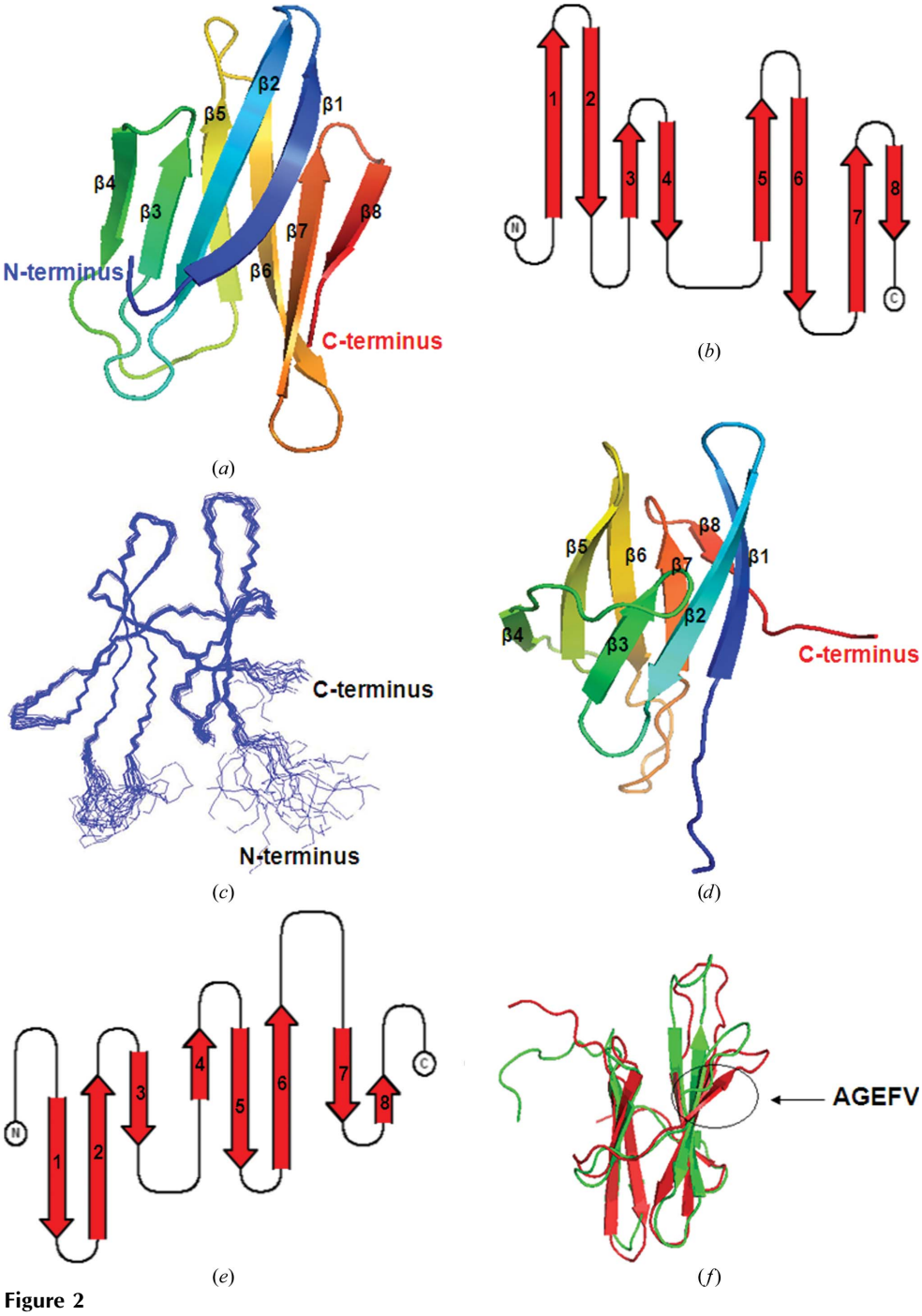

Figure 2
Three-dimensional structures of the FAIM-S NTD and CTD. (*a*) The structure of the FAIM-S NTD. Secondary structures are coloured from blue (N-terminus) to red (C-terminus) in a rainbow fashion; β-strands are numbered from 1 to 8. (*b*) Topology diagrams of the NTD. (*c*) The superimposition of 20 representative FAIM-S CTD structures. (*d*) Ribbon diagram of the CTD structure. Secondary-structure elements are coloured in the same way as for the NTD; β-strands are numbered from 1 to 8. (*e*) Topology diagrams of the CTD. (*f*) Structural superposition of the CTD from human (red) and mouse (green). The significant difference is shown by the black circle.

The crystal structure of the FAIM-S NTD was determined using the SAD method from a SeMet derivative diffracting to 1.76 Å resolution. The crystallographic refinement parameters are shown in Table 1. The crystal structure reveals that it is approximately spherical in shape, with dimensions of approximately 18 × 24 × 41 Å, and the peptide chain is organized into eight β-strands (β1, residues 4–12; β2, 15–23; β3, 30–34; β4, 37–42; β5, 50–56; β6, 61–70; β7, 74–81; β8, 84–88; Fig. 2*a*). The eight β-strands form two sheets (β1–β2–β3–β4 and β5–β6–β7–β8), which are canted with respect to each other by approximately 40°. The overall topology of the protein is simple and all β-strands are antiparallel. Successive β-strands are connected by 2–7 residue turns or loops (Fig. 2*b*).

The solution structure of the CTD domain was determined using inter-proton NOE-derived distance restraints in combination with dihedral angle restraints. 20 lowest-energy structures were selected to represent the CTD and are shown in Fig. 2(*c*), together with a ribbon diagram showing the secondary-structure elements (Fig. 2*d*). The structural statistics are shown in Table 2. The FAIM-S CTD contains amino-acid residues 91–179, which are renumbered 1–89 hereafter for convenience. The topology of the CTD is very similar to that of the NTD. It is

also nearly spherical in shape with dimensions of approximately 20 × 22 × 45 Å and comprises eight antiparallel β-strands (β1, residues 8–14; β2, 17–24; β3, 28–32; β4, 40–43; β5, 48–54; β6, 57–64; β7, 75–79; β8, 82–84; Fig. 2*d*). β1–β2–β3 form one β-sheet, while β4–β5–β6–β7–β8 form a second β-sheet. The two β-sheets are canted with respect to each other by approximately 30° (Fig. 2*e*).

In order to further analyze the structural features of the two domains, a *DALI* search (Holm & Sander, 1996) was applied using the FAIM-S NTD and CTD as models. A comparison with other known structures in the PDB gave 672 matches with *Z*-scores ranging from 2.0 to 4.2 for the NTD and 671 matches with *Z*-scores ranging from 2.0 to 4.4 for the CTD, apart from the mouse CTD (PDB entry 2kd2; Hemond *et al.*, 2009), which had a *Z*-score of 7.6 and an r.m.s.d. of 2.9 Å for the human NTD and a *Z*-score of 12.3 and an r.m.s.d. of 2.6 Å for the human CTD. The human CTD shares 81% sequence identity and a high similarity of structural packing with the mouse CTD. Superimposition revealed that the remarkable difference between them is residues Ala40-Gly41-Glu42-Phe43-Val44, which form a regular β-strand in the human CTD but form a loop in the mouse CTD (Fig. 2*f*).

3.2. Structural features of the FAIM-S NTD and CTD

The structure of the FAIM-S NTD is similar to that of the CTD, in which both antiparallel β-strands form two β-sheets. Residues Trp8, Ile19, Phe21, Val32, Ile40, Phe54, Ile65 and Leu79 in the NTD are involved in interfacial contacts (Fig. 3*a*). Among them, Trp8, Phe21, Phe54, Ile65 and Leu79 are strictly conserved, while Ile19 and Val32 are highly conserved (Fig. 1). The phenyl side chains of Phe21 and Phe54 interact with the side chains of Ile65 and Val32, respectively. The indole side chain of Trp8 also packs with the side chain of Leu79. These residues, in combination with Ile19 and Ile40, form a hydrophobic core which may contribute to the stability of the fold (Fig. 3*a*). Trp77 is also strictly conserved and is involved in the hydrogen-bonding network through water molecules.

In the structure of the FAIM-S CTD protein, Trp10, Leu12, Ile21, Val30, Phe52, Leu77, Val79 and Ile84 form a hydrophobic region to prevent movement of the two β-sheets. Trp10, Phe52 and Leu77 are strictly conserved, while the others are relatively conserved (Fig. 1). In particular, the phenyl side chain of Phe52 and the indole side chain of Trp10 pack closely with the side chains of Val30 and Leu77, respectively, which may be essential to maintain the structural stability in combination with other residues (Fig. 3*b*). Moreover, the two cysteines in the human FAIM-S CTD do not seem to play important roles in stabilization of the structure, which is consistent with the previous observation in murine FAIM-S CTD (Hemond *et al.*, 2009). Cys32 and Cys59 are buried in the hydrophobic region and cannot tolerate substitution by polar residues in the known sequences (Fig. 1). The two Cys residues are in the reduced state in the buffer in the NMR example, since no intramolecular disulfide bond is formed to stabilize the fold despite the relative positions of the Cys residues.

Table 2
Structural data statistics for the FAIM-S CTD.

Distance restraints	
Intra-residue unambiguous NOEs	1091
Sequential unambiguous NOEs	519
Medium-range unambiguous NOEs†	193
Long-range unambiguous NOEs‡	627
Total unambiguous NOEs	2430
Total ambiguous NOEs§	624
Dihedral angles (δ and ψ) (°)	62 (31/31)
R.m.s. from mean structure (Å)	
Backbone heavy atoms	
All residues	1.806 ± 0.545
Secondary structure	0.228 ± 0.035
All heavy atoms	
All residues	2.238 ± 0.540
Secondary structure	0.629 ± 0.049
Energy (kcal mol^{-1})	
Mean *AMBER* energy	−5050.56 ± 4.40
NOE distance restraints violation energy	26.69 ± 1.41
Torsion-angle restraints violation energy	0.553 ± 0.07
Restraint violations	
Distance (>0.3 Å)	0
Dihedral angle (>5°)	0
Ramachandran plot, residues in (%)	
Most favoured regions	85.1
Additional allowed regions	13.4
Generously allowed regions	0.9
Disallowed regions	0.6
Ramachandran plot (secondary structure), residues in (%)	
Most favoured regions	94.4
Additional allowed regions	5.5
Generously allowed regions	0.1
Disallowed regions	0

† Medium range represents two protons belonging to residues separated by no more than five amino acids. ‡ Long range represents protons belonging to residues separated by more than five amino acids in the primary sequence. § Ambiguous NOEs represent NOE-derived distance restraints that could be assigned to more than one pair of protons.

3.3. Oligomeric state of the FAIM-S NTD and CTD

In the process of protein purification, gel-filtration analysis was performed to characterize the oligomeric states of the two domains in solution. A comparison with molecular-weight calibrations using standard proteins indicated that the FAIM-S NTD exists as a dimer and that the CTD exists as a monomer (Fig. 4*a*). Cross-linking experiments followed by SDS–PAGE further confirmed that the NTD appears to form homodimers in solution, while the CTD appeared to be monomeric (data not shown). Moreover, analysis of the FAIM-S NTD structure further showed interaction between two NTD molecules related by a crystallographic twofold axis. The interface area between the two NTDs was calculated using *PISA* (Krissinel & Henrick, 2007) to be about 820 Å^2. Residue Lys37 in β4 of monomer *A* is positively charged and interacts with the corresponding negatively charged residue Glu43 in the loop connecting strands β4 and β5 of monomer *B* to form a salt bridge and *vice versa*. Besides this electrostatic interaction, hydrogen bonds between side chains and backbones of the residues on the contacting surface that form a network also contribute to the stability of the dimers. These residues are

mainly located in $\beta4$ in monomer *A* and $\beta4'$ in monomer *B* (Figs. 4*b* and 4*c*).

The electrostatic potential analysis indicated that $\beta4$ and $\beta5$ of the two NTD molecules form a noteworthy positively charged region in the dimer, suggesting that there may be negatively charged binding partners (Fig. 4*d*). Furthermore, the hydrophobic amino acids on the protein surface, Trp44, Met45, Phe46, Leu48, Val49, Gly50 and Thr53, are highly conserved among different organisms (Fig. 1) and are adjacent to the positively charged region (Fig. 4*e*), implying that they have important roles in binding the partners, if any, through hydrophobic interaction.

3.4. Interaction between the NTD and the CTD and its relation to the anti-apoptosis activity of FAIM-S

A previous chemical shift perturbation assay on murine FAIM-S indicated that the NTD interacts with the CTD, and Glu38, Arg110 and Asn123 were speculated to play key roles in mediating this interaction (Hemond *et al.*, 2009). In view of the high similarity in sequence and structure between the human and murine FAIM CTDs, as well as the strict conservation of all three of these residues, we hypothesized that the two domains of human FAIM-S can also interact with each other. We confirmed the interaction between the NTD and the CTD by co-immunoprecipitation (co-IP) of tagged proteins expressed in HEK 293T cells. Both of them were able to bind to each other but not to the control IgG (Fig. 5*a*), suggesting that the FAIM-S NTD and CTD perform interdomain communication. However, given that dimeric NTD was observed in solution and in the crystal structure, a contradiction seems to emerge because of a possible overlap between the interfaces of NTD–CTD interaction and the NTD dimer. In our previous experiment, full-length FAIM-S was temporarily stable despite being easy to degrade, making it possible to investigate how the intact protein behaves naturally. Gel-filtration analysis on a Superdex 75 high-performance column indicated that full-length FAIM-S exists as a monomer in solution, in which FAIM-S shows a similar chromatogram to the dimeric NTD (Fig. 5*b*). These data suggested that the FAIM-S NTD is prone to interact with the CTD rather than to form homodimers in the presence of CTD, despite the possibility that the structure of both free domains in solution may have a different conformation from that in the full-length protein.

A protein–protein docking model of the two domains using the *AutoDockTools*4 program (Goodsell & Olson, 1990; Morris *et al.*, 2009) was employed to help to further investigate the interaction between the NTD and the CTD (Fig. 5*c*). As shown in the docking model, the three most conserved residues, Glu38, Arg110 and Asn123, are located in the interface of NTD–CTD interaction and are close to residues such as Asp9 and Glu173 on the opposite molecule, hinting that they play key roles in interdomain communication. We next assessed whether these residues affect the interaction using a co-IP assay. We generated several mutation constructs, E38A in the NTD and R110A or N123A in the CTD, and then measured their immunoprecipitation together in HEK 293T cells. Compared with the interaction between wild-type NTD and CTD (Fig. 5*d*, lanes 2 and 4), the NTD–CTD interaction between the mutant and wild type decreased substantially (Fig. 5*d*, lanes 3, 5 and 6), and it decreased further when both the NTD and the CTD were mutated (Fig. 5*d*, lanes 7 and 8). Therefore, these data collectively reveal that Glu38, Arg110 and Asn123 have a notable effect on mediating the NTD–CTD interaction.

Apoptosis can be triggered by the death receptor-mediated extrinsic pathway and the mitochondrial intrinsic pathway (Hengartner, 2000). Induction of apoptosis by Bax is thought to caused by the insertion of Bax into the mitochondrial outer

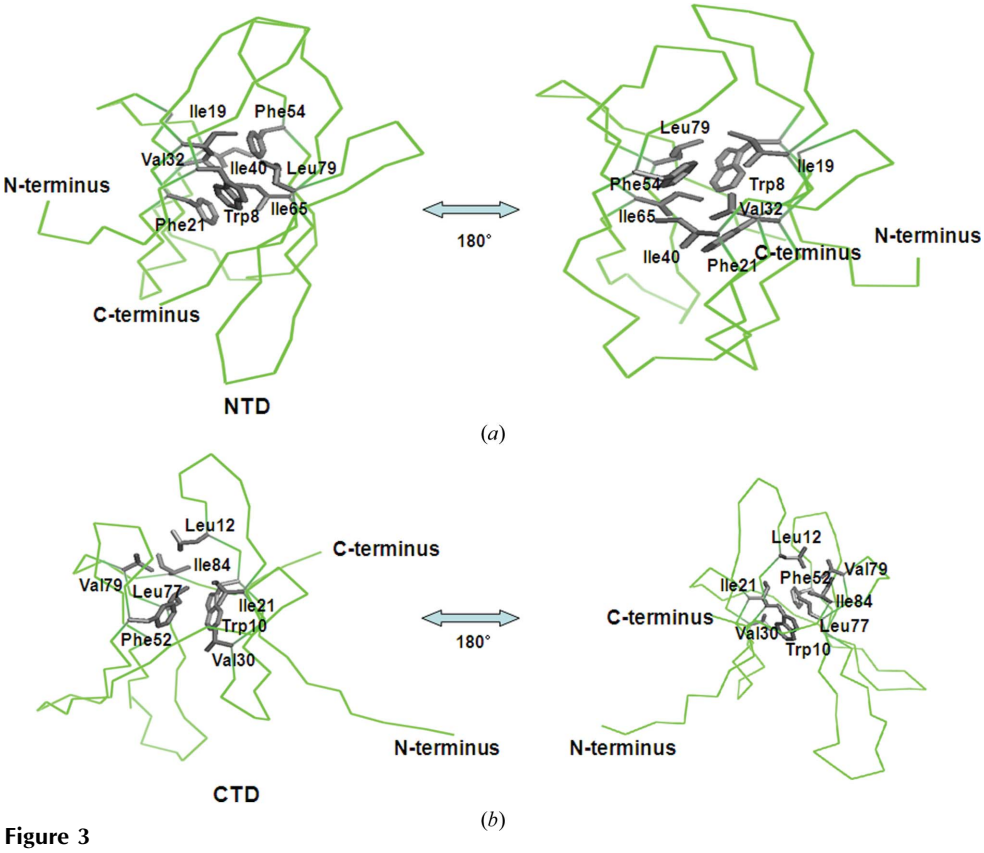

Figure 3
The hydrophobic core of the FAIM-S NTD and CTD. The residues involved in the hydrophobic core of the FAIM-S NTD (*a*) and CTD (*b*) are labelled and shown as a stick model.

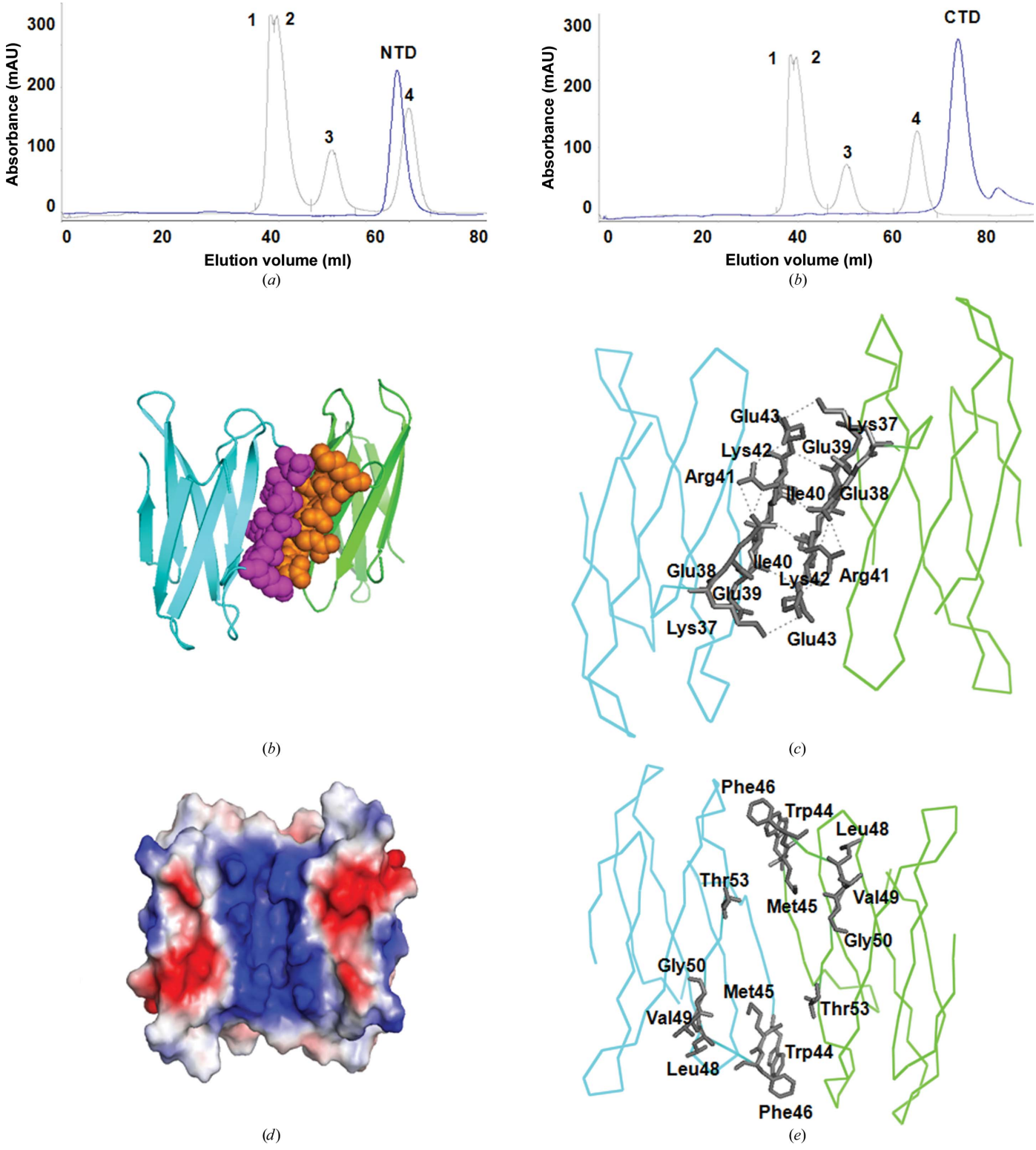

Figure 4
The oligomeric state of the FAIM-S NTD and CTD. (*a*) Gel-filtration analysis of the oligomeric state of the NTD and the CTD. The concentrated proteins were applied onto a Superdex 75 prep-grade column. The standard proteins used for molecular-weight calibrations were (1) thyroglobulin (670 kDa), (2) γ-globulin (158 kDa), (3) ovalbumin (44 kDa) and (4) myoglobin (17 kDa). (*b*) The two monomers are shown in cyan (molecule *A*) and green (molecule *B*). Residues located in the dimerization interface are shown as sphere representations and are coloured differently for each molecule (magenta for molecule *A* and orange for molecule *B*). (*c*) Detailed mechanism of dimer association. The molecules are coloured as in (*b*). The residues involved in the dimer association are labelled and shown as a stick model. Dashed lines indicate hydrogen bonds. (*d*) Surface model of the NTD dimer coloured according to the electrostatic potential. Positively charged residues are coloured blue, negatively charged residues are coloured red and neutral residues are coloured white. (*e*) The predicted residues may bind substrate through hydrophobic interaction. The molecules are coloured as in (*b*). The residues are labelled and shown as a stick model.

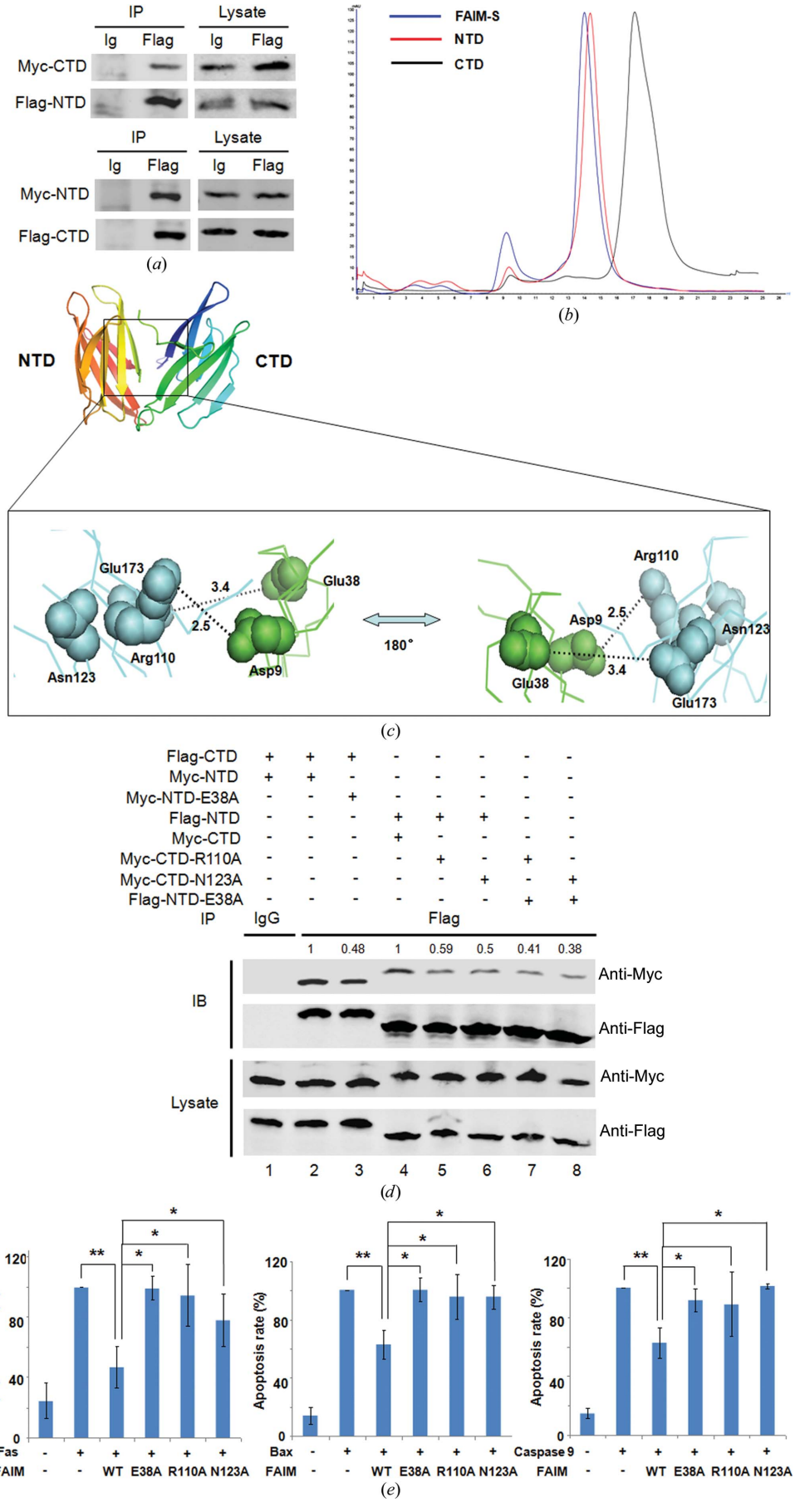

membrane, followed by the release of cytochrome *c* from mitochondria to bind to Apaf-1, resulting in the activation of caspase 9 (Budihardjo *et al.*, 1999). In contrast, apoptosis induced by overexpression of Fas in HEK 293T cells occurs through a caspase 9-independent pathway (Deveraux *et al.*, 1999). The apoptosis rate was analyzed by flow cytometry in cells transfected with FAIM-S together with Fas, Bax or caspase 9. The results revealed that FAIM-S was capable of suppressing Fas-induces, Bax-induced or caspase 9-induced apoptosis (Fig. 5*e*). These pro-apoptotic stimuli have been shown to initiate distinct apoptotic pathways involving the sequential activation of different caspases, which then converge at the downstream effector caspases,

Figure 5
Three critical residues are involved in the NTD–CTD interaction and affect the anti-apoptotic activity of FAIM-S. (*a*) Co-IP and immunoblot analysis of the interaction between the NTD and the CTD tagged by Flag or Myc in HEK 293T cells. (*b*) Chromatograms of full-length FAIM-S, the NTD and the CTD on a Superdex 75 high-performance column. The chromatograms are coloured blue, red and black, respectively. (*c*) Protein–protein docking model of the NTD–CTD interaction. The residues that may be involved in the interaction are marked in the NTD (green) and the CTD (cyan). Distances are given in Å. (*d*) Immunoassay of lysates of HEK 293T cells cotransfected with vectors expressing Flag-tagged or Myc-tagged NTD or CTD or their corresponding mutants including E38A, R110A and N123A. Quantitative comparison of the NTD–CTD interaction was indicated by density scanning of the blots, which was normalized to the interaction between wild-type NTD and CTD. (*e*) Effect of the three mutations on the anti-apoptotic activity of FAIM-S. HEK 293T cells were transfected with vectors expressing wild-type or mutants of FAIM-S together with Fas (left), Bax (middle) or caspase 9 (right). Flow cytometry was performed to measure apoptosis rates. * indicates a significant difference at $p < 0.05$ and ** a highly significant difference at $p < 0.01$. The data shown are representative of at least three independent experiments.

particularly caspase 3. Our study indicates that FAIM-S may function at the downstream of Fas, Bax and caspase 9 to inhibit caspase 3 activity and ultimately to decrease cell apoptosis.

Next, we investigated whether the interaction between the NTD and the CTD impacts on the anti-apoptosis activity of FAIM-S. The three mutations mentioned above, E38A, R110A and N123A, were introduced into full-length FAIM-S. In contrast to the evident anti-apoptotic activity of wild-type FAIM-S, expression of these mutations showed an indistinct inhibitory effect on apoptosis induced by different apoptotic stimuli (Fig. 5*e*). Allowing for the fact that these mutations partly impair the interaction between the NTD and the CTD, the data suggested that the anti-apoptotic activity of FAIM-S might be associated with the NTD–CTD interdomain interaction.

In the present work, we have determined the first crystal structure of the human FAIM-S NTD and the NMR solution structure of the human FAIM-S CTD. These structures showed that the FAIM-S NTD has a similar conformation to the CTD, both of which are composed of eight antiparallel β-strands forming two sheets. Structural and gel-filtration analyses revealed that the full-length FAIM-S and the CTD exist as monomers in solution, while the NTD exists as dimers, which may be related to their different biological functions under diverse physiological conditions. We modelled the interaction between the NTD and the CTD and confirmed using a co-IP assay that Glu38, Arg110 and Asn123 play considerable roles. All of these mutations also disturb the anti-apoptosis activity of FAIM-S, suggesting a potential correlation between the NTD–CTD interaction and the anti-apoptosis activity of FAIM-S. The structural information and functional experiments will provide an insight into the precise mechanism of this apoptosis-inhibitory molecule.

3.5. Accession codes

The atomic coordinates reported in this paper have been deposited in the Protein Data Bank (http://www.pdb.org; PDB entry 3mx7 for the NTD and 2kw1 for the CTD). Chemical shift assignments have been deposited in the Biological Magnetic Resonance Data Bank with accession No. 17864.

We would like to thank Professor Yicheng Dong for helpful discussions. Data were collected at Beijing Synchrotron Radiation Facility and Shanghai Synchrotron Radiation Facility. This work was supported by grants from the NSFC 30930020, the National High Technology and Development Program of China 973 program (No. 2010CB911800) and the International Centre for Genetic Engineering and Biotechnology (ICGEB; Project No.CRP/CHN09-01) to XZ and from the 863 program (No. 2006AA02A323) to CJ.

References

Alderson, M. R., Tough, T. W., Davis-Smith, T., Braddy, S., Falk, B., Schooley, K. A., Goodwin, R. G., Smith, C. A., Ramsdell, F. & Lynch, D. H. (1995). *J. Exp. Med.* **181**, 71–77.

Baker, N. A., Sept, D., Joseph, S., Holst, M. J. & McCammon, J. A. (2001). *Proc. Natl Acad. Sci. USA*, **98**, 10037–10041.

Brunner, T., Mogil, R. J., LaFace, D., Yoo, N. J., Mahboubi, A., Echeverri, F., Martin, S. J., Force, W. R., Lynch, D. H., Ware, C. F. & Green, D. R. (1995). *Nature (London)*, **373**, 441–444.

Budihardjo, I., Oliver, H., Lutter, M., Luo, X. & Wang, X. (1999). *Annu. Rev. Cell Dev. Biol.* **15**, 269–290.

Chinnaiyan, A. M., O'Rourke, K., Yu, G.-L., Lyons, R. H., Garg, M., Duan, D. R., Xing, L., Gentz, R., Ni, J. & Dixit, V. M. (1996). *Science*, **274**, 990–992.

Cornilescu, G., Delaglio, F. & Bax, A. (1999). *J. Biomol. NMR*, **13**, 289–302.

Delaglio, F., Grzesiek, S., Vuister, G. W., Zhu, G., Pfeifer, J. & Bax, A. (1995). *J. Biomol. NMR*, **6**, 277–293.

Deveraux, Q. L., Leo, E., Stennicke, H. R., Welsh, K., Salvesen, G. S. & Reed, J. C. (1999). *EMBO J.* **18**, 5242–5251.

Duggan, B. M., Legge, G. B., Dyson, H. J. & Wright, P. E. (2001). *J. Biomol. NMR*, **19**, 321–329.

Edgar, R. C. (2004). *Nucleic Acids Res.* **32**, 1792–1797.

Emsley, P., Lohkamp, B., Scott, W. G. & Cowtan, K. (2010). *Acta Cryst.* D**66**, 486–501.

Fisher, G. H., Rosenberg, F. J., Straus, S. E., Dale, J. K., Middleton, L. A., Lin, A. Y., Strober, W., Lenardo, M. J. & Puck, J. M. (1995). *Cell*, **81**, 935–946.

Goodsell, D. S. & Olson, A. J. (1990). *Proteins*, **8**, 195–202.

Gouet, P., Courcelle, E., Stuart, D. I. & Métoz, F. (1999). *Bioinformatics*, **15**, 305–308.

Grillot, D. A., Merino, R., Pena, J. C., Fanslow, W. C., Finkelman, F. D., Thompson, C. B. & Nunez, G. (1996). *J. Exp. Med.* **183**, 381–391.

Güntert, P., Mumenthaler, C. & Wüthrich, K. (1997). *J. Mol. Biol.* **273**, 283–298.

Hemond, M., Rothstein, T. L. & Wagner, G. (2009). *J. Mol. Biol.* **386**, 1024–1037.

Hengartner, M. O. (2000). *Nature (London)*, **407**, 770–776.

Herrmann, T., Güntert, P. & Wüthrich, K. (2002). *J. Biomol. NMR*, **24**, 171–189.

Holm, L. & Sander, C. (1996). *Science*, **273**, 595–603.

Johnson, B. A. (2004). *Methods Mol. Biol.* **278**, 313–352.

Kaku, H. & Rothstein, T. L. (2009*a*). *J. Immunol.* **183**, 1667–1674.

Kaku, H. & Rothstein, T. L. (2009*b*). *J. Immunol.* **183**, 5575–5581.

Krissinel, E. & Henrick, K. (2007). *J. Mol. Biol.* **372**, 774–797.

Laskowski, R. A., Rullmannn, J. A., MacArthur, M. W., Kaptein, R. & Thornton, J. M. (1996). *J. Biomol. NMR*, **8**, 477–486.

Li, G., Qu, L., Meng, G., Bai, X., Dai, K. & Zheng, X. (2010). *Acta Cryst.* F**66**, 935–937.

Morris, G. M., Huey, R., Lindstrom, W., Sanner, M. F., Belew, R. K., Goodsell, D. S. & Olson, A. J. (2009). *J. Comput. Chem.* **30**, 2785–2791.

Murshudov, G. N., Skubák, P., Lebedev, A. A., Pannu, N. S., Steiner, R. A., Nicholls, R. A., Winn, M. D., Long, F. & Vagin, A. A. (2011). *Acta Cryst.* D**67**, 355–367.

Nicholson, D. W. *et al.* (1995). *Nature (London)*, **376**, 37–43.

Oshimi, Y., Oda, S., Honda, Y., Nagata, S. & Miyazaki, S. (1996). *J. Immunol.* **157**, 2909–2915.

Otwinowski, Z. & Minor, W. (1997). *Methods Enzymol.* **276**, 307–326.

Perrakis, A., Morris, R. & Lamzin, V. S. (1999). *Nature Struct. Biol.* **6**, 458–463.

Petersen, I., Bujard, M., Petersen, S., Wolf, G., Goeze, A., Schwendel, A., Langreck, H., Gellert, K., Reichel, M., Just, K., du Manoir, S., Cremer, T., Dietel, M. & Ried, T. (1997). *Cancer Res.* **57**, 2331–2335.

Schneider, T. J., Fischer, G. M., Donohoe, T. J., Colarusso, T. P. & Rothstein, T. L. (1999). *J. Exp. Med.* **189**, 949–956.

Schneider, T. J., Grillot, D., Foote, L. C., Núñez, G. E. & Rothstein, T. L. (1997). *J. Immunol.* **159**, 4834–4839.

Segura, M. F., Sole, C., Pascual, M., Moubarak, R. S., Perez-Garcia, M. J., Gozzelino, R., Iglesias, V., Badiola, N., Bayascas, J. R., Llecha, N., Rodriguez-Alvarez, J., Soriano, E., Yuste, V. J. & Comella, J. X. (2007). *J. Neurosci.* **27**, 11228–11241.

Smyth, M. J., Sutton, V. R., Kershaw, M. H. & Trapani, J. A. (1996). *Transplantation*, **62**, 1529–1532.
Sole, C., Dolcet, X., Segura, M. F., Gutierrez, H., Diaz-Meco, M. T., Gozzelino, R., Sanchis, D., Bayascas, J. R., Gallego, C., Moscat, J., Davies, A. M. & Comella, J. X. (2004). *J. Cell Biol.* **167**, 479–492.
Suda, T., Okazaki, T., Naito, Y., Yokota, T., Arai, N., Ozaki, S., Nakao, K. & Nagata, S. (1995). *J. Immunol.* **154**, 3806–3813.
Terwilliger, T. C. (2000). *Acta Cryst.* D**56**, 965–972.
Terwilliger, T. C. & Berendzen, J. (1999). *Acta Cryst.* D**55**, 849–861.
Tewari, M., Quan, L. T., O'Rourke, K., Desnoyers, S., Zeng, Z., Beidler, D. R., Poirier, G. G., Salvesen, G. S. & Dixit, V. M. (1995). *Cell*, **81**, 801–809.
Trauth, B. C., Klas, C., Peters, A. M., Matzku, S., Möller, P., Falk, W., Debatin, K. M. & Krammer, P. H. (1989). *Science*, **245**, 301–305.
Van Parijs, L., Refaeli, Y., Abbas, A. K. & Baltimore, D. (1999). *Immunity*, **11**, 763–770.
Wang, J., Homer, R. J., Chen, Q. & Elias, J. A. (2000). *J. Immunol.* **165**, 4051–4061.
Yonehara, S., Ishii, A. & Yonehara, M. (1989). *J. Exp. Med.* **169**, 1747–1756.
Zhong, X., Schneider, T. J., Cabral, D. S., Donohoe, T. J. & Rothstein, T. L. (2001). *Mol. Immunol.* **38**, 65–72.